Experiment and Theoretical Study of Poly(vinyl pyrrolidone)-controlled Gold Nanoparticles

ARTICLE *in* THE JOURNAL OF PHYSICAL CHEMISTRY C · OCTOBER 2008

Impact Factor: 4.77 · DOI: 10.1021/jp803935y

4 AUTHORS, INCLUDING:

Xuchuan Jiang
Monash University (Australia)
104 PUBLICATIONS **4,466** CITATIONS
SEE PROFILE

Aibing Yu
University of New South Wales
621 PUBLICATIONS **11,660** CITATIONS
SEE PROFILE

Experiment and Theoretical Study of Poly(vinyl pyrrolidone)-controlled Gold Nanoparticles

L. Kemal,[†] X. C. Jiang,[†,‡] K. Wong,[†] and A. B. Yu*[,†]

School of Materials Science and Engineering, University of New South Wales, Sydney, NSW 2052, Australia and School of Materials and Metallurgy, Northeastern University, Shenyang, 110004, P. R. China

Received: November 26, 2007; Revised Manuscript Received: August 4, 2008

This paper reports a facile synthesis method for shape control of gold nanoparticles by treating an aqueous solution of chloroauric acid with sodium citrate and poly(vinyl pyrrolidone) (PVP). By such an environmentally friendly method, gold nanoparticles were prepared with different morphologies including spheres, rods, and worm-like nanoparticles. Two possible growth mechanisms were proposed in the formation of wormlike particles: from spherical colloids to nanorods, and from nanorods to worm-like particles by stacking faults or by rods conjunction. It was found that the PVP plays a key role in the formation of nanostructures by acting as reducing agent, stabilizer, and surface capping agent. Density function theory (DFT) is applied to quantify the binding energies of PVP with different gold crystal surfaces (i.e., 100, 110, and 111). Such a DFT approach, facilitated by transmission electron microscopy and ultraviolet−visible spectroscopy characterizations, will be useful for fundamental understanding of the growth mechanism of gold nanorods.

1. Introduction

Nanoparticles have attracted considerable attention because of their specific properties and potential applications.[1] In particular, metallic nanoparticles (e.g., gold, silver, and copper) have become increasingly attractive due to their unique optical, electronic, magnetic, and chemical properties. Such functional properties have driven them for a wide range of applications in optical imaging in medical and biological areas,[2] nanodevices,[3] catalysts,[4] optical sensors,[5−7] and surface-enhanced Raman scattering (SERS).[8,9]

The optical properties of metal nanoparticles are strongly dependent upon their particle characteristics (shape, size, and their distributions). Many attempts have been made to control the shape and size during synthesis, particularly for anisotropic metal nanostructures (e.g., rods, wires, plates, and disks), for desirable functional properties, such as hydrochemical synthesis,[10] electrochemical method,[11] biological reduction,[12] microwave-polyol heating process,[13] liquid crystal template,[14] and seed-mediated method.[10,15] A successful case in preparation of metal nanorods was reported by both Murphy and El-Sayed groups.[10,15] The investigators have made significant improvements through a seed-mediated approach to synthesize gold and silver nanorods/nanowires in the presence of cetyltrimethylammonium bromide (CTAB) and have shown that the CTAB could form double layers to control anisotropic growth and that the unique plasmon resonance of gold and silver nanorods could be finely tuned by changing their aspect ratios. Another sample is the exploration of applications as interconnections toward future nanocircuits and nanodevices, multiple-pod gold nanostructures were recently achieved in aqueous $HAuCl_4$−CTAB solution by Chen, et al.[16] Such branched particles (e.g., tripods and tetrapods) were characterized with multiple growth directions, and the formation of such multipod structures might lower the energy of the system by breaking the cubic symmetry of the face-centered-cubic (fcc) lattice. Such multiarmed structures are frequently observed in semiconductor materials.[17−21]

It is of significant importance to understand the mechanisms governing particle growth in nanotechnology. In most cases, the morphologies of these thermodynamically unfavorable particles have been explained by the particular reaction environment in which they are synthesized. The mechanisms mainly fall into two categories, one in which the presence and orientation of stacking faults on {111} facets or twin planes in these fcc metals direct particle morphology[22,23] and the other where chemically or physically adsorbed molecules kinetically regulate the growth of specific crystal surfaces.[4−6,10,15] A typical example is the shape control of gold and silver nanoparticles using surfactant, poly(vinyl pyrrolidone) (PVP), as a capping agent,[4] which can selectively interact with gold planes (e.g., 111, 100, and 110), and thus resulted in different metal nanostructures including nanorods, nanowires, nanoplates, and nanocubes. Recently, Ravishankar and co-workers[24] proposed that the oriented attachment of Au{111} facets could result in the growth of gold nanorods via {111} fusion. However, many methods are difficult to develop further as a general theory for interpreting formation mechanisms of anisotropic nanoparticles. To date, the choice of synthesis methods and the use of surfactants are empirical. Developing a more quantitative method for better understanding the growth of anisotropic nanoparticles is still a challenging task.

In this work, we report a facile method to control the shape of gold nanoparticles through a two-step heating process in the presence of PVP in aqueous solution. The formation of particles with different shapes can be controlled by finely adjusting the experimental parameters, such as concentration, surfactants, reaction time, and temperature. An attempt is also made to understand the growth mechanism of the nanostructures (e.g., rods) by the density functional theory (DFT) method, and other advanced experimental techniques including transmission electron microscopy (TEM), high-resolution TEM (HRTEM), and ultraviolet−visible (UV−vis) photospectrometry.

* To whom correspondence should be addressed. Tel: +61-2-93854429, Fax: +61-2-93855956, Email: a.yu@unsw.edu.au.
[†] University of New South Wales.
[‡] Northeastern University.

10.1021/jp803935y CCC: $40.75
Published on Web 09/12/2008

2. Experimental Work

2.1. Chemicals. All chemicals, including hydrochloroauric acid ($HAuCl_4 \cdot 3H_2O$, 99.9%), sodium citrate (99.5%), poly(vinyl pyrrolidone) (PVP, 99%, with mean molecular weight 55, 000), cetyltrimethylammonium bromide (CTAB), and bis(2-ethylhexyl) sulfosuccinate (AOT) were purchased from Sigma−Aldrich and were used as received. All solutions were freshly prepared with Milli-Q water, and glassware was cleaned with aqua regia, thoroughly rinsed with Milli-Q water, and dried prior to use.

2.2. Synthesis of Gold Nanoparticles. ***Worm-like Nanoparticles.*** To optimize experimental conditions such as concentrations, reaction time, and temperature, many tests have been carried out. In a typical procedure, three steps were involved. First, the solution containing $HAuCl_4$ and PVP was mixed in a vial, and the total volume was fixed at 20 mL, in which the final concentrations were 5.0×10^{-4} M and 4.0×10^{-3} M for $HAuCl_4$ and PVP, respectively. The pH value of such a mixture was measured around 5. Second, the mixture was preheated at 50 °C for ∼30 min, and the light yellow color of the solution remained in this treatment. Finally, the vial containing the preheated solution was placed into hot water for reflux heating at 95 °C. After ∼5 min, an appropriate amount of sodium citrate (the molar ratio of citrate to $AuCl_4^-$ ions was 3) was added to the solution, followed by continuous reflux heating. Upon the addition of reducing agents (e.g., sodium citrate), the solution turned color from yellow to ruby red and, finally, dark purple.

Spherical Nanoparticles. By adjusting the experimental parameters (e.g., reaction temperature) of the PVP−$AuCl_4^-$ system, spherical gold nanoparticles could be prepared. Briefly, three steps were involved. The former two steps are the same as those in the synthesis of gold worm-like particles. There is a slight difference in the third step. The preheated PVP−$AuCl_4^-$ solution (at 50 °C for ∼30 min) was not directly put into hot water but bathed first with cold water (∼5 °C) for 3 h before reflux heating at 95 °C. The solution turned color from bright yellow to ruby red but not purple.

2.3. Characterization. The microstructure of the as-synthesized gold worm-like particles was characterized under a Philips CM200 field emission gun TEM, operated at an accelerating voltage of 200 kV. The specimen was prepared by dropping the particle suspension onto the Formvar-coated copper grid and then naturally dried in air. UV−vis absorption spectra were obtained on a CARY 5G UV−visible spectrophotometer (Varian) with a standard 1 cm quartz cell. Normally, 3 mL of solution containing gold nanoparticles was placed into the standard quartz cell for each measurement. The data for particle size distribution were automatically collected using the Image Processing and Analysis Program (ImageJ, v1.37, 2006).

2.4. Density Functional Theory (DFT) Calculation. The binding energy (BE) of PVP with gold crystalline surfaces (i.e., 110, 100, and 111) was calculated based on DFT using DMol3. The spin unrestricted geometry optimization and energy calculation steps were performed using the generalized gradient approximation scheme with the Perdew Burke and Ernzerhof (PBE) exchange-correlation function. A DNP (double numerical extra polarization) basis set that accounts for polarization functions was used with the ECP (effective core potentials) pseudopotential. The tolerances for energy, gradient, and displacement convergence for geometry optimization are 2×10^{-3} Ha/Å, 1×10^{-5} Ha, and 0.005 Å, respectively. The model was simulated as a periodic supercell with at least 10.0 Å of vacuum gap between the upper most portions of the model with the top of the simulation cell. The Brillouin zone integration was performed using a $5 \times 5 \times 1$ Monkhorst−Pack grid.

3. Results and Discussion

3.1. Worm-like Gold Nanoparticles. The synthesis of gold nanoparticles was achieved by a combined preheating (50 °C) and refluxing process (95 °C). These two-step heating processes aimed at separating the particle nucleation and growth as far as possible for obtaining particles with controlled shape/size. The microstructure of gold nanoparticles was characterized by TEM technique. Figure 1A shows the TEM images of nanoparticles that are composed of ∼65% spheres (∼10 nm in diameter), ∼30% short nanorods, and a few worm-like particles, together with some gold dots (2−3 nm in diameter) after reflux heating at 95 °C for 10 min. A 20 min difference in reflux heating resulted in a distinct change in particle morphology. This can be seen from Figure 1B that over 50% spherical particles grew bigger to rod-like particles (∼60 nm in length and ∼20 nm in diameter), along with spherical particles. As the reflux heating was extended up to 45 min or more (e.g., 60 min), almost all the particles grew longer (Figure 1, panels C and D). In the meantime, those small gold dots nearly disappeared with longer reflux heating (e.g., 60 min). The crystallization of these nanoparticles was further identified by the selected area electron-diffraction (SAED) pattern shown in the inset of Figure 1D. Those electron diffraction rings could be assigned to (111), (200), (220), (311), and (222) planes of fcc Au. On the basis of the above TEM analysis, the growth of the worm-like nanoparticles was presented as a function of the reflux heating time under the conditions considered.

To trace the particle growth, the corresponding optical absorption of gold nanoparticles was measured and is shown in Figure 2. It was seen that the absorption intensity of the four investigated samples decreased a little at the peak centered at $\lambda_{max} = 526$ nm, but the curve tail progressively increased beyond 620 nm with the increase of reflux heating time. Over a short refluxing period (e.g., 10 min), a single plasmon band centered at $\lambda_{max} = 526$ nm was observed (curve a), indicating that the spherical particles were dominant in the product; this was confirmed by our TEM observations (Figure 1A). When the refluxing time increased, a second peak centered at around $\lambda_{max} = 748$ nm (curve c) or $\lambda_{max} = 791$ nm (curve d) was observed in the samples corresponding to 45 and 60 min, respectively. In analyzing the optical properties, we intended to assign the second plasmon band to two possibilities: (i) the wormlike particles themselves due to their anisotropic morphologies and (ii) the existence of solution-stable aggregates of gold nanoparticles, although they are hard to clearly distinguish. Meanwhile, it was noted that the absorption intensity in the longitudinal surface plasma ranging from 700 to 800 nm was weaker than those obtained from the gold nanorods.[10,25] This is due to the worm-like shape and/or the wide size distribution of particles (Figure 1, panels C and D).

The microstructure of gold particles was further checked by HRTEM technique. Figure 3 shows the HRTEM images of gold nanoparticles of different shapes. One short nanorod was identified as a twinning structure and is shown in Figure 3B, which was also confirmed by the spots of (200) and (222) marked as m1-n1 vs m2-n2 in the SAED pattern (inset of Figure 3B). The lattice fringes continuously extended to the whole particles. A closer inspection revealed that the lattice fringes of the nanorod has an interplanar distance of ∼0.285 nm, corresponding to Au{110} facets. This indicated that the Au{110} facets are edge-on bounded, and the rod grows along the direction of [001] as marked by arrowhead in Figure 3B. In the previous study, Wang et al.[26] suggested that those facets enclosing the short nanorods were identified with the dominant

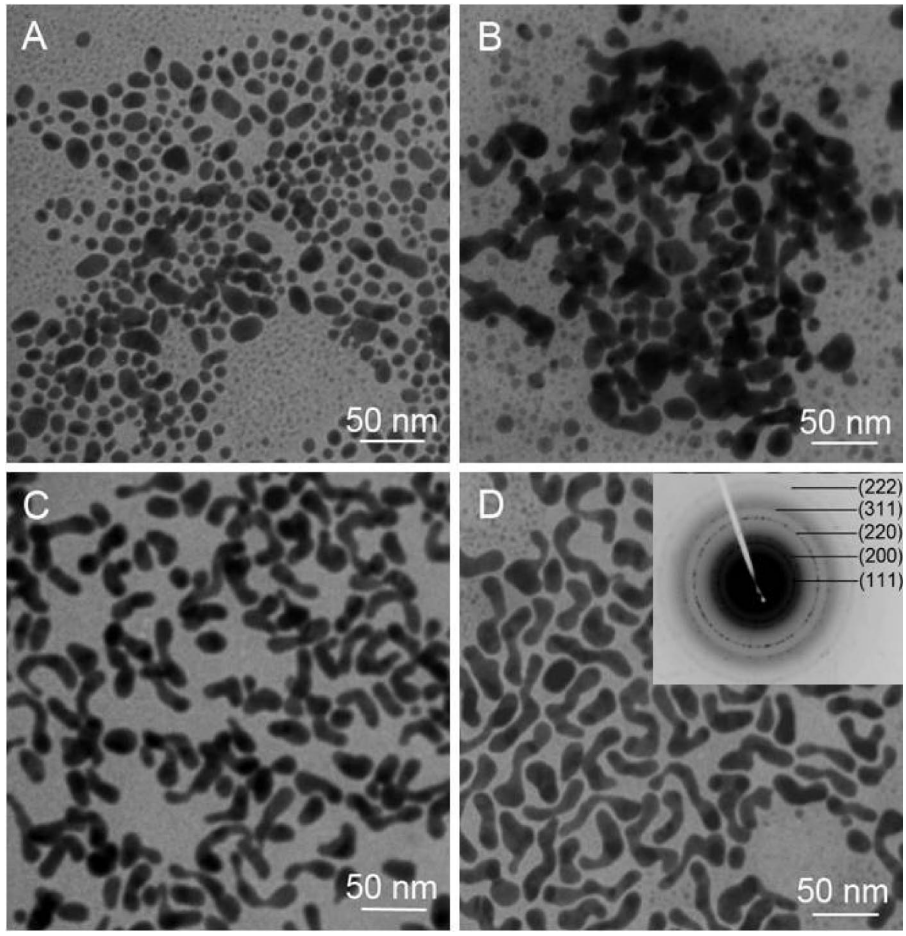

Figure 1. The TEM images of gold worm-like nanoparticles prepared under different reflux heating time at 95 °C: (A) 10 min, (B) 30 min, (C) 45 min, and (D) 60 min. The inset of panel D, showing the electron diffraction pattern of nanoparticles, corresponds to (111), (200), (220), (311), and (222) planes of the face-centered-cubic gold.

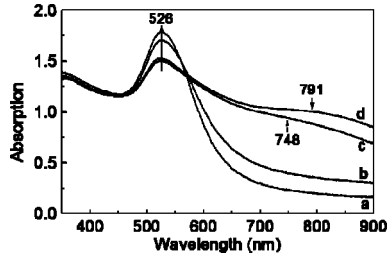

Figure 2. The UV−vis spectra (a−d) corresponding to the samples shown in Figure 1, panels A−D.

sides being {110} planes and with the growth direction of a gold nanorod being <001>, and the ends of the nanorods were terminated by {111} planes with smaller areas. These findings could be supportive for our observations on the nanorods with edge-on {110} planes on the rod and {111} planes at the tip (Figure 3D). Moreover, we found that the starting end of the gold nanoparticles was slightly wider than the terminating end, thus it looked like a needle (Figure 3B). The formation of needle-like particles was caused by two possibilities: one is that the Au{111} facets with narrower lattice spacing (~0.25 nm) become dominant at the terminated end, and another is that the twinned structure or stacking faults led to the formation of needle-like particles. Such structure is a bit different from gold nanorods with same width in the entire particle as reported by Murphy and Natan.[10] The investigators also proposed that the cross section of gold nanorods capped by CTAB is pentagonal and that each end is composed of five triangular faces that are Au{111}. The sides of the rods are not as well-defined; either Au{110} or Au{100} faces or both.

Figure 3, panels E and F, shows HRTEM images indicating that the worm-like particles are of polycrystalline structure. This is also confirmed by the corresponding electron diffraction patterns (insets of Figure 3, panels D−F), in which the diffraction spots are difficult to index because they might originate from different domains of a single worm-like particle. As a result, it is difficult to well define to which facets the sides of these polycrystalline structures belong. The formation of such worm-like structures was probably caused by two growth processes: from spherical colloids to short nanorods, and then the nanorods grew into worm-like particles by stacking faults or by the conjunction of the nanorods. The first growth process from spherical colloids to nanorods can be readily explained by both experiments and theoretical methods (e.g., DFT). However, the mechanism for the second growth process of the formation of worm-like particles is not very clear. It is believed that more work needs to be performed to understand the formation of polycrystalline worm-like gold particles.

3.2. Effects of Experimental Parameters. ***Reaction Temperature.*** Three mixtures containing both PVP and $AuCl_4^-$ ions were separately preheated at 40, 60, and 70 °C for 30 min, before further reflux heating at 95 °C. Lower (<30 °C) and higher (>80 °C) temperatures were not tested in this work. The other experimental conditions were kept the same as those preheated at 50 °C. The TEM images in Figure 4 show that the as-prepared particles were elliptical (~20%) and were worm-like (~80%)

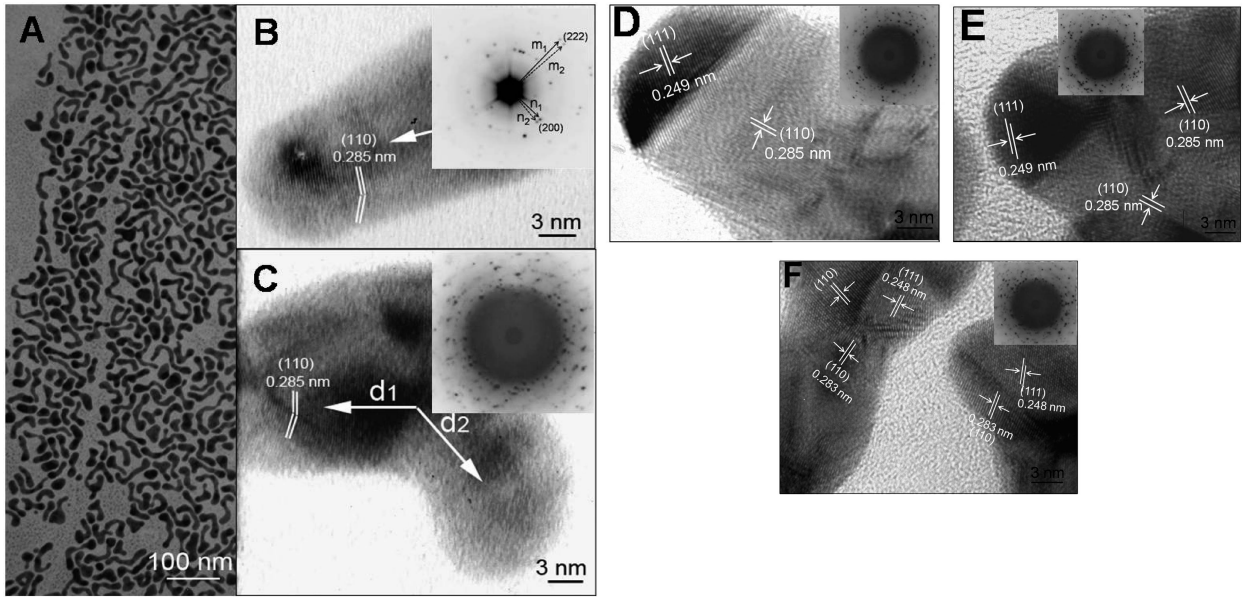

Figure 3. (A) TEM image of gold worm-like nanoparticles; (B) HRTEM image of a short nanorod with twinning structure; (C) an L-shaped gold particle with the interplanar distance around 0.285 nm, corresponding to Au{110} facets; (D) the dominant {111} facets at the terminated end of rod-like particles; (E) stacking faults at the junction part of one worm-like particle; and (F) polycrystalline worm-like nanoparticles.

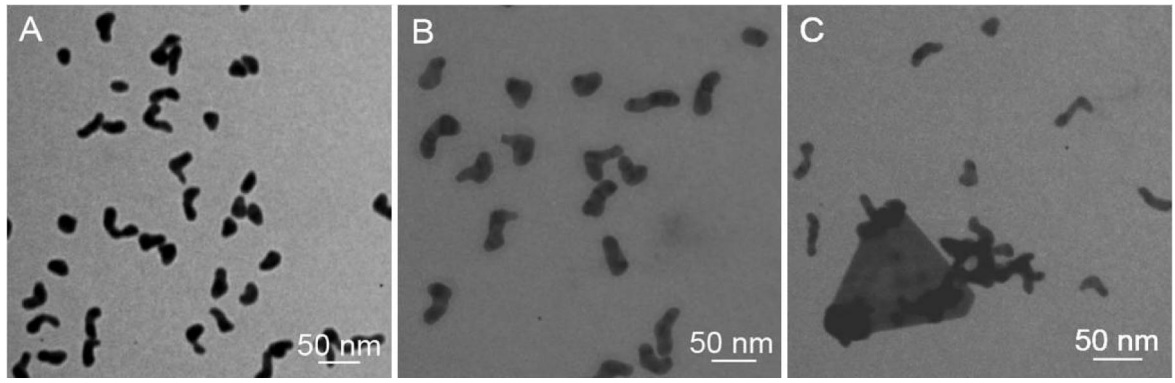

Figure 4. The TEM images of gold nanoparticles prepared under the same preheating time (30 min) but different temperatures: (A) 40, (B) 60, and (C) 70 °C.

for the sample that was preheated at 40 °C for 60 min (Figure 4A). With increasing preheating temperature, most of the gold particles grew into the worm-like shape, as shown in Figures 4B (60 °C) and 4C (70 °C). The TEM analysis suggested that the preheating treatment in the range of 40−70 °C had a slight influence on the formation of worm-like gold particles.

The effect of the preheating temperature on particle shape and size was further examined, focusing on low temperatures (e.g., 5 °C). Four vials containing PVP−$AuCl_4^-$ solution were first preheated at 50 °C for different times (e.g., 10, 30, 45, and 60 min), and then all samples were immersed in cold water (5 °C). After bathed in such cold water for ∼3 h, the 4 samples were placed into hot water (95 °C) for reflux heating upon the addition of sodium citrate. The light-yellow solution gradually turned ruby over a period of 60 min, indicating that gold colloids formed. Figure 5 shows that almost all the particles were spherical in shape, but no worm-like particles were observed in all four samples. This is probably due to the surface activity of gold atoms being greatly reduced in such cold water, which would hinder the preferential growth on one crystal surface, subsequently leading to the formation of spherical particles. A close look by HRTEM shows that the gold colloids are of twinned structure, which might lower the energy of the system by creating an initial electronic asymmetry.[22b]

Further evidence shows that the effect of low temperature on particle shape and size could be seen from the size distribution shown in Figure 5, panels AA−DD. These gold nanoparticles were almost spherical in shape, and their average sizes were estimated to be 9.8 ± 2.8 nm (AA), 8.1 ± 2.5 nm (BB), 7.9 ± 2.9 nm (CC), and 13.6 ± 3.5 nm (DD), based on the calculation using a computer program. The size over 20 nm could be originated from the attachment of two or more particles, as shown in Figures 5, panels CC and DD. However, no worm-like particles were formed in such a reaction system even if it was heated over 60 min at 95 °C. This was also supported by the corresponding optical absorption shown in the UV−vis spectra (Figure 6). Only a single plasmon band centered at ∼525 nm was observed. The slight difference in UV−vis spectra was due to the different size distributions. As opposed to the above two-step heating processes, the mixed system containing PVP, $AuCl_4^-$, and sodium citrate was directly heated to 95 °C without any preheating treatment. Figure 7 shows that the final product was composed of particles with diverse sizes and shapes (e.g., rods, triangles, and spheres), but no worm-like nanoparticles were formed. The result suggested that the preheating treatment affected the shape and growth of gold particles.

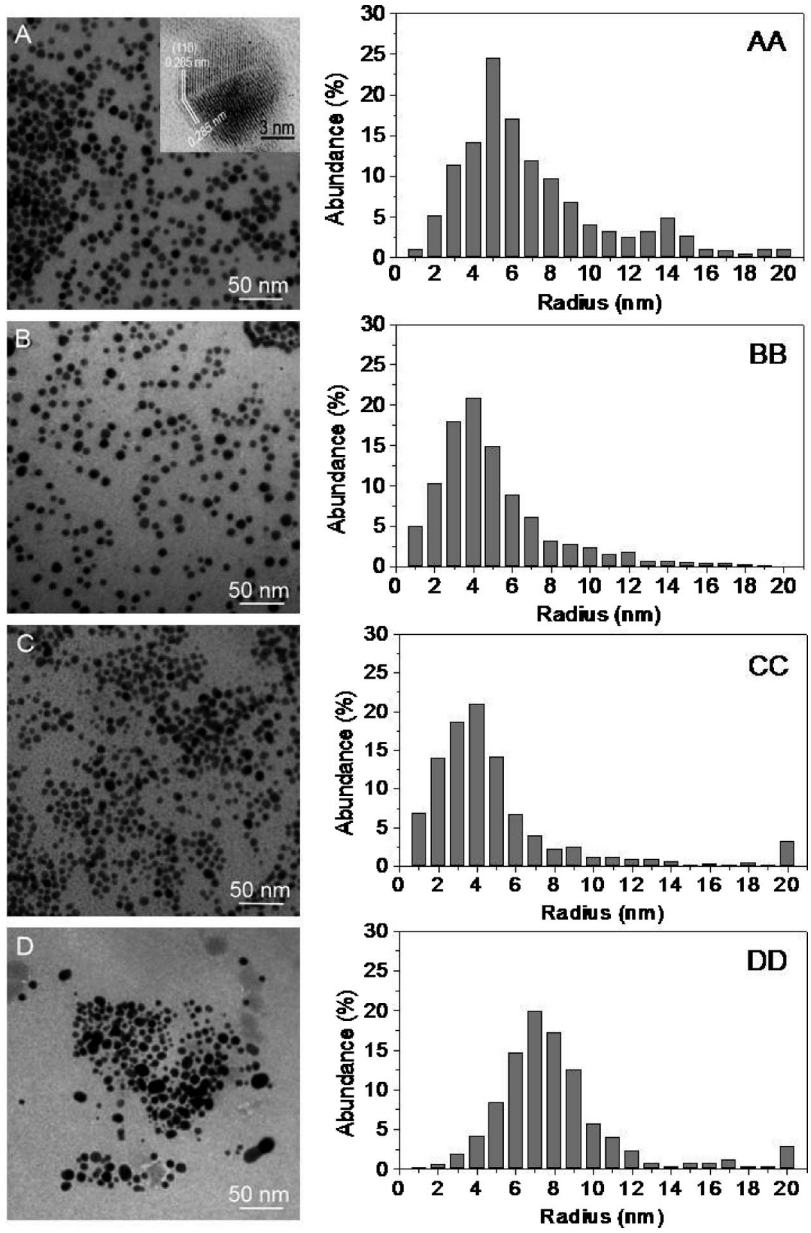

Figure 5. The TEM images of gold nanoparticles prepared by preheating at 50 °C for different times—(A) 10, (B) 30, (C) 45, and (D) 60 min—followed by immersing vials into cold water (~5 °C), to investigate the influence of temperature on the seed and hence the particle shape and size. The inset of Figure 5A shows that spherical particles are also twinned structures with edge-on {110} planes. The histograms illustrate the corresponded particle size distributions (AA−DD).

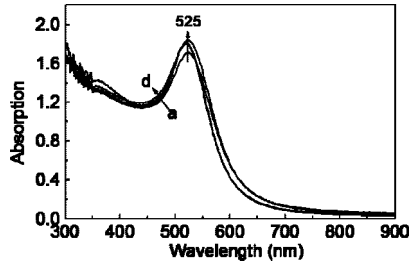

Figure 6. The UV−vis spectra corresponding to four samples shown in Figure 5, in which the surface plasmon resonance is centered at around 525 nm.

Surfactants of AOT and CTAB. In comparison, two other surfactants (AOT and CTAB) were tested for shape control. Both of them were commonly employed in the synthesis of metal nanoparticles (e.g., Au, Ag, and Cu) with shape control. For instance, AOT molecules have been used for making silver nanodiscs by forming reverse micelles in isooctane.[22] Our recent studies have demonstrated that the AOT molecules played a key role in the growth of silver nanoplates by selectively adsorbing on Ag planes (111, 110, and 100).[27] Similarly, the CTAB molecules have also been used for preparing silver triangles and gold nanorods through selective adsorption on the crystal surface.[10,15,23] In this work, we intended to replace PVP with AOT or CTAB but maintain the other experimental conditions (e.g., concentration, reaction time, and temperature) for testing their capabilities in shape control. When the samples were preheated at 50 °C for 30 min, no color change happened in both the AOT−$AuCl_4^-$ and the CTAB−$AuCl_4^-$ systems, indicating that both AOT and CTAB had no ability to reduce $AuCl_4^-$ ions to Au atoms under the reported conditions. Subsequent reflux heating at 95 °C and addition of sodium citrate led to solution color change from light yellow to purple, revealing that gold particles were formed in such systems.

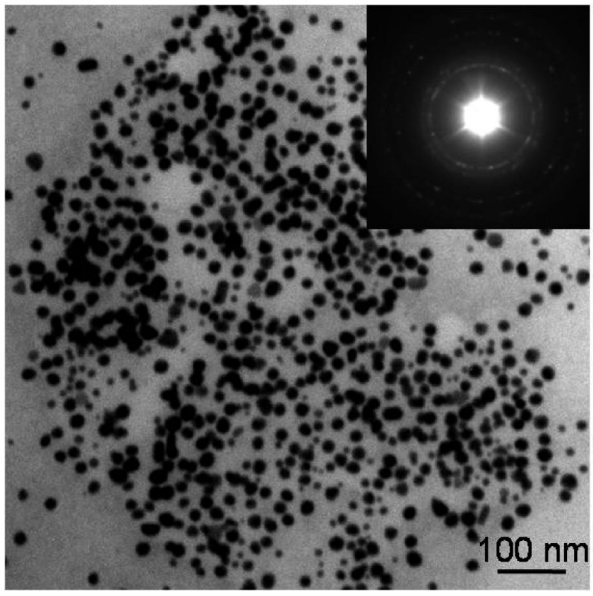

Figure 7. The TEM image of gold nanoparticles obtained without preheating treatment.

The microstructure of the product was further characterized. Figure 8A shows the TEM images of the particles that almost aggregated, and they are difficult to clearly distinguish in the shape and size. This is different from our recent study on the synthesis of silver nanodiscs using AOT as a stabilizer, where nearly monodispersed silver nanoplates were observed.[27] In the case of using CTAB, the gold nanoparticles show diverse morphologies (e.g., triangles, rods, and spheres) (Figure 8B). Despite the outcome, the diffraction rings recorded in the SAED patterns (inset of Figure 8, panels A and B) suggested the nanoparticles are of crystalline nature. The above TEM analysis proved that different surfactants exhibit different capabilities in shape and size control.

PVP−$AuCl_4^-$ and Citrate−$AuCl_4^-$ Systems. Two reaction systems, that is, PVP−$AuCl_4^-$ and citrate−$AuCl_4^-$, were separately examined to understand the influence of PVP and citrate ions on particle growth. In the first system, three vials containing PVP−$AuCl_4^-$ solution were heated at 50 °C for different times (e.g., 10, 30, and 60 min). Figure 9A shows one typical TEM image of the sample that was heated over a period of 60 min. The particles were small (2−3 nm in diameter), but they were still of crystalline structure, as confirmed by the corresponding electron diffraction rings (inset of Figure 9A). The optical absorption was recorded, and an enlarged part of the plasmon band centered at ~541 nm is shown in the inset of Figure 9C. The UV−vis spectra (curves a−c) show that the absorption intensity increased as a function of heating time, indicating more gold particles formed with time. The weak absorption implied that the concentration of gold colloids is low in the solution. The formation of gold colloids without addition of sodium citrate suggested that PVP is capable of reducing $AuCl_4^-$ ions to Au atoms.

This is not the first report of the ability of PVP to reduce $AuCl_4^-$ in aqueous solution. Hoppe et al.[4b] demonstrated the preparation of gold and silver using PVP to reduce metal ions and to provide a narrow-size distribution for silver colloids, but various shapes and sizes have been obtained for gold nanoparticles including spheres, plates, rods, and others. The possible mechanisms were proposed by the authors to explain the reduction step: direct hydrogen abstraction induced by the metal ion and/or reducing action of macroradicals formed during degradation of the polymer. Initial formation of the macroradicals might be associated with the metal-accelerated decomposition of low amounts of peroxides present in the commercial polymer. Xia et al.[4c] reported that PVP could reduce Ag^+ ions to prepare circular and triangular Ag nanoplates, but it needed heating at 60 °C over a long time (>40 min). The difference in reduction capability is because the gold salt has a higher reduction potential (~0.2 V) than silver salt; hence, PVP is barely able to reduce silver at a higher temperature or with a longer time than gold. In our study, a third function of PVP was used to reduce gold ions in the preheating stage (50 °C), and the resulting gold colloids are 2−3 nm in diameter (Figure 9A). This is different from that reported by Hoppe,[4b] who used solely PVP but obtained wide size distributions of gold particles. These colloids could further serve as nucleation sites for forming big gold nanoparticles when the citrate ions were added. Here the gold particles showing different morphologies were probably caused by the use of two reducing agents (PVP and citrate ions) that could result in two nucleation and growth processes: (i) the colloids reduced by PVP served as nucleation sites for those newly reduced Au atoms growth, and (ii) a part of gold ions were directly reduced by citrate ions and then nucleated and grew bigger. These two growth processes would result in spheres or nanorods formation. For the formation of worm-like particles, two growth mechanisms might be involved in this study: from spherical colloids to nanorods, and from nanorods to worm-like structures by stacking faults or by conjunction of rods. However, the detailed mechanism is still not clear. It is believed that more work needs to be performed to understand the particle growth and shape control.

Compared to the PVP−$AuCl_4^-$ system, the citrate−$AuCl_4^-$ solution gradually turned to ruby when it was heated at 50 °C for ~20 min. Figure 9B shows the TEM image of the particles that are nearly spherical in shape and with an average size of ~25 nm in diameter. The corresponding electron diffraction rings (inset of Figure 9B) revealed that they are of crystalline structure under the reported conditions. Moreover, the optical absorption was clearly stronger than those obtained from the PVP−$AuCl_4^-$ system (Figure 9D), indicating that bigger size and/or higher concentration of gold particles were formed in the citrate−$AuCl_4^-$ system under the similar conditions. This suggested that both PVP and citrate ions have the reducing ability, but PVP is relatively weak in reducing $AuCl_4^-$ ions to Au atoms.

3.3. Particle Growth Mechanism. The TEM analysis (Figures 1 and 3) indicated that the particles formed rod-like and worm-like structures. At the preheating stage (50 °C), some $AuCl_4^-$ ions could be partially reduced by PVP to form small gold dots (Figure 9A). The PVP-capped gold dots could provide nucleation sites for further growth of gold particles when citrate ions were added. By reflux heating at 95 °C, there was a competition between the PVP adsorption/desorption and the newly formed gold atoms grown on the gold dots, which would result in a possible oriented growth in the formation of anisotropic gold nanostructures (e.g., rods). The selective adsorption of PVP on the gold crystal surfaces (111, 110, and 100) could lead to anisotropic geometry. This is similar to the previous studies in preparation of fcc gold and silver nanoparticles. For example, Ravishankar et al.[24] demonstrated that the oriented attachment of gold nanoparticles took place in {111} facets by fusing together to form a nanorod or nanowire. Such a fusion in {111} facets represented a preferential removal of the capping molecules from these crystalline planes. Another representative sample in this field to use PVP for shape control

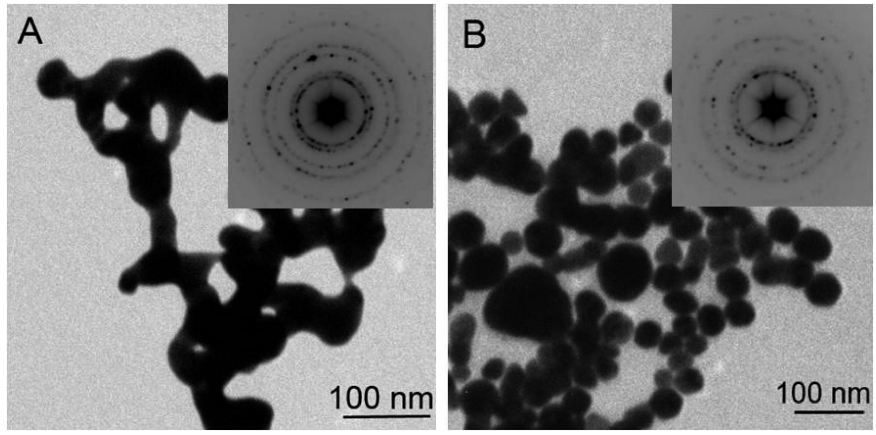

Figure 8. The TEM images of Au nanoparticles prepared using different surfactants: (A) AOT and (B) CTAB. The electron diffraction patterns (insets of A and B) indicating that the gold particles are of crystalline nature.

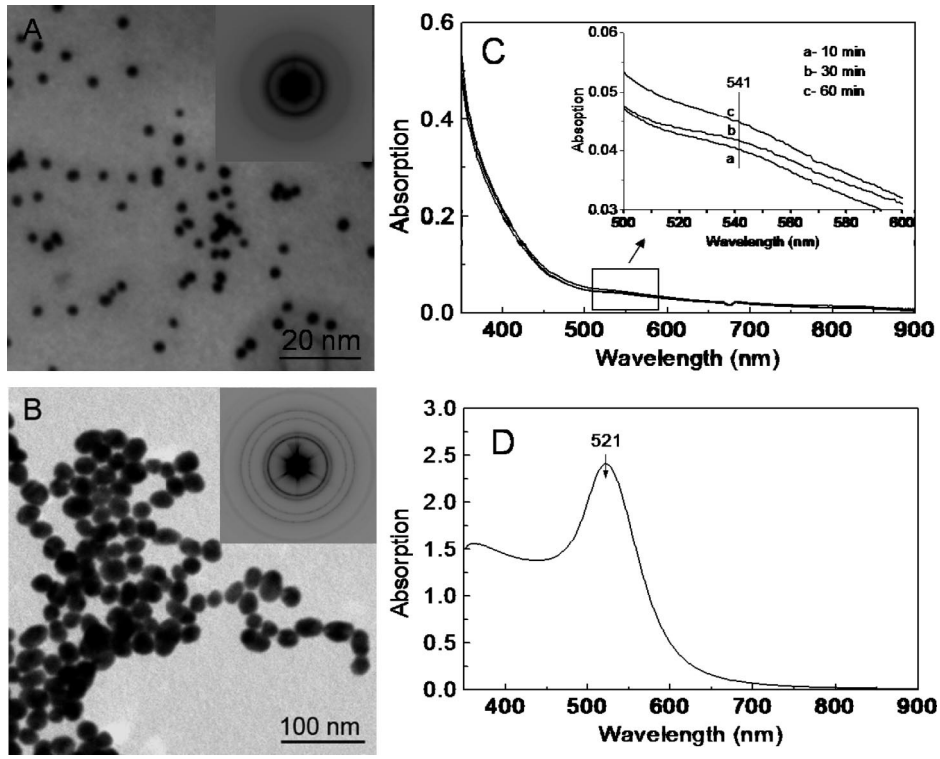

Figure 9. (A) TEM image and the corresponding electron diffraction pattern of gold dots obtained from the preheated PVP−$AuCl_4^-$ solution at 50 °C for 60 min; (B) TEM image and the electron diffraction pattern of gold nanoparticles obtained from the preheated citrate−$AuCl_4^-$ solution at 50 °C for ∼20 min; (C and D) the corresponding UV−vis spectra of gold particles.

of metal particles was reported by Xia and co-workers.[4] The investigators reported that the PVP-coated silver nanoparticles of different morphologies (rods, wires, plates, and cubes) could be finely controlled by adjusting experimental parameters, especially the molar ratio of PVP to silver salt.

In spite of the development of various synthesis methods, it is still challenging to systematically control the shape of nanoparticles. This is due to the limited understanding of the particle growth mechanism. To overcome the problem, theoretical calculations based on molecular dynamics (MD) and DFT methods have become more attractive. They can be used to calculate the surface energy, interaction energy, and binding energy of metal and surrounding molecules, which is useful for understanding particle growth at a molecular scale. Recently, the MD method was used in our work to explain the shape control of silver nanoplates in the presence of AOT molecules. In this AOT−Ag system, the interaction energies between AOT and different Ag surfaces were calculated as 460.1, 323.4, and 249.9 kcal mol^{-1} for Ag{111}, Ag{110}, Ag{100} respectively. The stronger interaction of AOT−Ag{111} planes restrict the growth on this plane, and hence the other two planes grow faster, which benefits the formation of silver nanoplates.[27]

The DFT approach has also been used to calculate binding energy (BE) between metal surfaces and adsorbed atoms or molecules. The BE represents the attractive or repulsive force of the adsorbed atoms or molecules on certain metal plane and subsequently affects the growth orientation of metal particles. In the present PVP−Au system, the theoretical lattice parameter for Au was calculated to be 4.201 Å, which is consistent with that of Boon et al.[29] for a similar system. However, it is known that the Au lattice parameter calculated using the Perdew−Wang-like exchange-correlation functionals is ∼2.5% larger than the experimental lattice parameter of 4.08 Å.[30] Figure 10 shows that the PVP molecule interacts with each of the gold crystalline

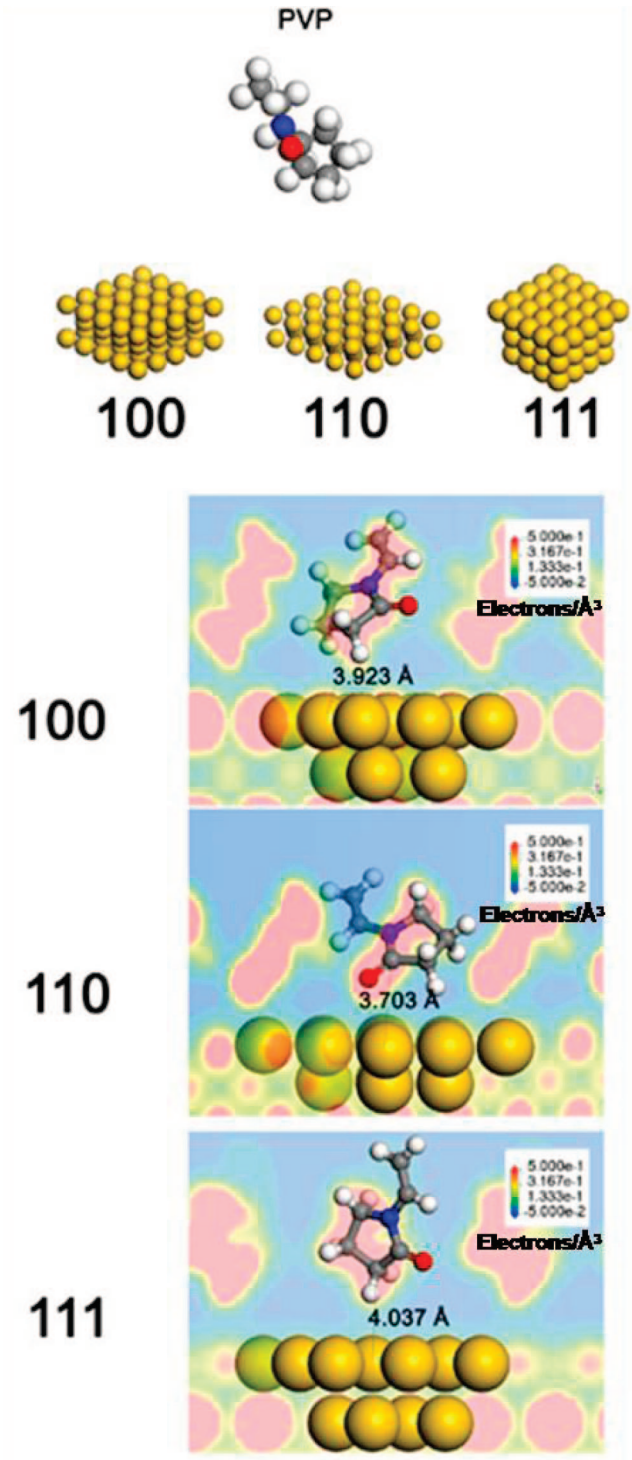

Figure 10. (A) DFT calculation showing that PVP interacts with each gold crystalline plane (i.e., 111, 110, and 100); (B) the planar electron density profile of the PVP/Au system, indicating the electrostatic interaction between PVP and Au. The atoms are colored as follows: Au (yellow), H (white), O (red), N (blue), and C (gray).

planes (i.e., 111, 110, and 100). The preferential adsorption of PVP molecules on gold crystal planes was determined by the BE. Such BE was calculated by the following equation:

$$\Delta E_{BE} = E_{A-B} - (E_A + E_B)$$

where E_{A-B}, E_A and E_B were the BEs of the gold plane with PVP (A−B), the isolated gold plane (A), and the isolated PVP (B), respectively. The BE between PVP and the gold crystallographic planes was calculated as −0.0531, −0.0425, and 0.0197 eV for {111}, {100}, and {110}, respectively. In principle, the higher the BE, the stronger the adsorption strength. Thus, the PVP adsorbed strongly on the {110} planes, whereas on the {111} and {100} planes the PVP molecules were slightly repelled. This could also be confirmed by the shorter distance between Au{110} and the closest carbon atom in PVP (3.703 Å), in comparison to 3.923 Å for Au{100} and 4.037 Å for Au{111}. The closest C atom to Au was chosen for distance measurement because this atom better resembled a pivot for PVP, and the electron density resided in the C, O, and N atoms of PVP. From this knowledge, the spatial and geometric reconfigurations of the polymer backbone can be determined by regions of high electron density. On the contrary, the H atom had a smaller atomic radius and had only one bond attached to it, as it had more degrees of freedom. Thus, if one was to define H as the reference point for distance measurement, the result may not accurately represent the real environment. To overcome this problem, the C atom was chosen as the reference point. The results showed that PVP prefers to adsorb on {110} planes and blocks the growth on these planes, therefore it is not surprising to see the edge-on {110} planes of gold nanorods (Figure 3B). However, we need to point out that such DFT calculations still have difficulty explaining the formation of polycrystalline gold wormlike particles at this stage due to the limitation in large-scale calculations. It is believed that more work is needed to understand the particle growth.

Figure 10 shows the planar electron density profile of the PVP−Au system, indicating the electrostatic interactions of PVP with Au surfaces. It can be seen from this plot that there is an electrostatic interaction region between PVP and Au with a tentative redistribution of electrons among this interface. The BE for PVP adsorption on Au{111} and Au{100} planes suggested that there is a repulsive barrier at these interfaces. Such repulsion effect may induce the growth along these two planes, particularly along Au{111} planes, as it is more energetically favorable. Therefore, the Au{110} planes on particle sides are not surprising in this case (Figure 3B). It is of importance to mention that PVP in an aqueous environment reorganizes itself into a complex network of polymer backbones stabilized by electrostatic interactions. The irregular arrangement of polymers required simulation models to be simplified. Thus, the PVP molecules are positioned in such a way that the electrostatic interaction in the polymer backbone will be reflected throughout the periodic boundary cell. In light of this fact, we believed that the qualitative prediction of PVP BE trends was reasonable. However, the magnitude of the BE may only reflect one particular arrangement of PVP on Au. Therefore, the BE of the PVP molecules on Au results in the formation of gold nanorods. A distinct phenomenon differs from the usual formation of truncated octahedron for free clusters caused by the surface energies in bare gold.[31] Furthermore, the formation of worm-like particles rather than longer nanorods was observed from TEM and HRTEM images (Figures 1C−D and 3C−F). This is probably caused by two growth processes: from spherical colloids to nanorods, and from nanorods to worm-like nanostructures by stacking faults or by conjunction of short nanorods. The former one can be understood by DFT simulations. However, the detailed mechanism for the latter process is difficult to explain by our DFT simulations. Therefore, more work needs to be conducted for understanding the growth of worm-like particles.

4. Conclusions

We have demonstrated the synthesis of PVP-controlled gold nanoparticles by a combined experimental and theoretical study. These gold nanoparticles were obtained with different morphologies—including spheres, rods, and worm-like structures—by varying experimental parameters. The multishaped particles were probably caused by the separated nucleation and growth procedures: (i) the colloids reduced by PVP could serve as nucleation sites for forming bigger particles, and (ii) a part of gold ions were directly reduced by citrate and then nucleated and grew bigger. In particular, the formation of worm-like structures might be explained by two growth processes: from spherical colloids to nanorods, and then from nanorods to worm-like particles by stacking faults or by conjunction of nanorods. In the synthesis, PVP can function as a surface capping agent, a stabilizer, and a reducing agent for gold. The DFT was applied to calculate the binding energies between PVP and gold surfaces, which provides some molecular information for understanding the growth of gold nanorods. However, such DFT simulations are difficult to explain the formation of worm-like nanostructures in this study. It is believed that more work needs to be performed to understand particle growth and shape control.

Acknowledgment. We gratefully acknowledge the financial support from the Australia Research Council (ARC) through the ARC Centre of Excellence for Functional Nanomaterials, Natural Science Foundation of China (NSF50671019), and China Postdoctoral Science Foundation (No. 2005038252). X.J. gratefully thanks Dr. W. Yang for the help in taking the HRTEM images and also thanks Dr. A. Brioude (University of Lyon, France) for valuable discussions.

References and Notes

(1) (a) *Nanoscale Materials in Chemistry*, Klabunde, K. J., Ed.; John Wiley & Sons: New York, 2001. (b) Hsu, H. Y. *NNIN REU Research Accomplishment* **2004**, 68–69.

(2) (a) Xia, Y.; Halas, N. J. *MRS Bull.* **2005**, *30*, 338–348. (b) Salem, A. K.; Searson, P. C.; Leong, K. W. *Nat. Mater.* **2003**, *2*, 668–671.

(3) Yun, Y. J.; Park, G.; Ah, C. S.; Park, H. J.; Yun, W. S.; Ha, D. H *Appl. Phys. Lett.* **2005**, *87*, 2331101–2331103.

(4) (a) Sun, Y.; Xia, Y. *Science* **2002**, *298*, 2176–2178. (b) Hoppe, C. E.; Lazzari, M; Pardiñas-Blanco, I.; López-Quintela, M. A *Langmuir* **2006**, *22*, 7027–34. (c) Washio, I.; Xiong, Y.; Yin, Y.; Xia, Y. *Adv. Mater.* **2006**, *18*, 1745–1749.

(5) Jin, R.; Cao, Y.; Mirkin, C. A.; Kelly, K. L.; Schatz, G. C.; Zheng, J. G. *Science* **2001**, *294*, 1901–1903.

(6) (a) Obare, S. O.; Hollowell, R. E.; Murphy, C. J. *Langmuir* **2002**, *18*, 10407–10410. (b) Lin, S. Y.; Liu, S. W.; Lin, C. M.; Chen, C. H. *Anal. Chem.* **2002**, *74*, 330–335. (c) Kim, Y. J.; Johnson, R. C.; Hupp, J. T. *Nano Lett.* **2001**, *1*, 165–167. (d) Gooding, J.; Hibbert, D. B.; Yang, W. *Sensors* **2001**, *1*, 75–90. (e) Yang, W.; Gooding, J.; Hibbert, D. B. *J. Electroanal. Chem.* **2001**, *516*, 10–16. (f) Jensen, T. R.; Malinsky, M. D.; Haynes, C. L.; van Duyne, R. P. *J. Phys. Chem. B* **2000**, *104*, 10549–56.

(7) Jiang, X. C.; Yu, A. B. *Langmuir* **2008**, *24*, 4300–9.

(8) (a) Hu, H.; Aizpurua, J.; Kall, M.; Apell, P. *Phys. Rev. E* **2000**, *62*, 4318. (b) Garcia-Vidal, F. J.; Pendry, J. B. *Phys. Rev. Lett.* **1996**, *77*, 1163.

(9) (a) Inoue, M.; Ohtaka, K. *J. Phys. Soc. Jpn.* **1983**, *52*, 3853. (b) Liver, N.; Nitzan, A.; Gersten, J. *Chem. Phys. Lett.* **1984**, *111*, 449. (c) Boyd, G. T.; Rasing, T.; Leite, J. R. R.; Shen, Y. R. *Phys. Rev. B* **1984**, *30*, 519. (d) Zeman, E. J.; Schatz, G. C. *J. Phys. Chem.* **1987**, *91*, 634.

(10) (a) Jana, N. R.; Gearheart, L.; Murphy, C. J. *J. Phys. Chem. B* **2001**, *105*, 4065–4067. (b) Murphy, C. J.; Jana, N. R. *Adv. Mater.* **2002**, *14*, 80–82. (c) Sau, T. K.; Murphy, C. J. *Langmuir* **2005**, *21*, 2923–2929. (d) Murphy, C. J.; Jana, N. R. *Adv. Mater.* **2002**, *14*, 80–82. (e) Gao, J. X.; Bender, C. M.; Murphy, C. J. *Langmuir* **2003**, *19*, 9065–70. (f) Brown, K. R.; Walter, D. G.; Natan, M. J. *Chem. Mater.* **2002**, *12*, 306. (g) Johnson, C. J.; Dujardin, E.; Davis, S. A.; Murphy, C. J.; Mann, S. *J. Mater. Chem.* **2002**, *12*, 1765–1770.

(11) Zhou, M.; Chen, S.; Zhao, S.; Ma, H. *Chem. Lett.* **2005**, *34*, 1670–1671.

(12) Shankar, S. S.; Rai, A.; Ankamwar, B.; Singh, A.; Ahmad, A.; Sastry, M. *Nat. Mater.* **2004**, *3*, 482–488.

(13) Tsuji, M.; Matsumoto, K.; Nishizawa, Y.; Tsuji, T. *Mater. Lett.* **2005**, *58*, 2326–2330.

(14) Yamamoto, M.; Kashiwagi, Y.; Sakata, T.; Hirotaro, M.; Nakamoto, M. *Chem. Mater.* **2005**, *17*, 5391–5393.

(15) (a) Nikoobakht, B.; El-Sayed, M. A. *Chem. Mater.* **2003**, *15*, 1957–1962. (b) Burda, C.; Chen, X.; Narayanan, R.; El-Sayed, M. A. *Chem. Rev.* **2005**, *105*, 1025–1102. (c) El-Sayed, M. A. *Acc. Chem. Res.* **2001**, *34*, 257–264.

(16) Chen, S.; Wang, Z. L.; Ballato, J.; Foulger, S. H.; Carroll, D. L *J. Am. Chem. Soc.* **2003**, *125*, 16186–16187.

(17) Jun, Y. W.; Lee, S. M.; Kang, N. J.; Cheon, J. *J. Am. Chem. Soc.* **2001**, *123*, 5150–5151.

(18) (a) Manna, L.; Scher, E. C.; Alivisatos, A. P. *J. Am. Chem. Soc.* **2000**, *122*, 12700–12706. (b) Peng, X. *Adv. Mater.* **2003**, *15*, 459–463.

(19) (a) Manna, L.; Milliron, D. J.; Meisel, A.; Scher, E. C.; Alivisatos, A. P. *Nat. Mater.* **2003**, *2*, 382–385. (b) Peng, Z. A.; Peng, X. *J. Am. Chem. Soc.* **2001**, *123*, 183–184.

(20) Jun, Y. W.; Jung, Y. Y.; Cheon, J. *J. Am. Chem. Soc.* **2002**, *124*, 615–619.

(21) (a) Iwanaga, H.; Fujii, M.; Ichihara, M.; Takeuchi, S. *J. Cryst. Growth* **1994**, *141*, 234–238. (b) Tang, C. C.; Fan, S. S.; de la Chapelle, M. L.; Li, P. *Chem. Phys. Lett.* **2001**, *333*, 12–15. (c) Roy, V. A. L.; Djurisic, A. B.; Chan, W. K.; Gao, J.; Lui, H. F.; Surya, C. *Appl. Phys. Lett.* **2003**, *83*, 141–143.

(22) (a) Peréz-Juste, J.; Pastoriza-Santos, I.; Liz-Marzán, L. M.; Mulvaney, P. *Coord. Chem. Rev.* **2005**, *249*, 1870–1901. (b) Pérez-Juste, J.; Liz-Marzán, L. M.; Carnie, S.; Chan, D. Y. C.; Mulvaney, P. *Adv. Funct. Mater.* **2004**, *14*, 571–579. (c) Mulvaney, P.; Pérez-Juste, M.; Giersig, L. M.; Liz-Marzán, C. P. *Plasmonics* **2006**, *1*, 61–66.

(23) (a) Germain, V.; Li, J.; Ingert, D.; Wang, Z. L.; Pileni, M. P *J. Phys. Chem. B* **2003**, *107* (34), 8717–8720. (b) Maillard, M.; Giorgio, S.; Pileni, M. P. *Adv. Mater.* **2002**, *14*, 1084–1086. (c) Lofton, C.; Sigmund, W. *Adv. Funct. Mater.* **2005**, *15*, 1197–1208. (d) Chen, S.; Carroll, D. L. *Nano Lett.* **2002**, *2*, 1003–1007.

(24) Halder, A.; Ravishankar, N. *Adv. Mater.* **2007**, *19*, 1854–1858.

(25) (a) Brioude, A.; Jiang, X. C.; Pileni, M. P. *J. Phys. Chem. B* **2005**, *109*, 13138–13142. (b) Jiang, X. C.; Pileni, M. P. *Colloid Interface A* **2007**, *295*, 228–232. (c) Jiang, X. C.; Brioude, A.; Pileni, M. P. *Colloid Interface Sci A* **2006**, *277*, 201–206.

(26) (a) Wang, Z. L.; Mohamed, M. B.; Link, S.; El-Sayed, M. A. *Surf. Sci.* **1999**, *440*, L809–L814. (b) Dai, Z. R.; Sun, S.; Wang, Z. L. *Surf. Sci.* **2002**, *505*, 325–335.

(27) (a) Jiang, X. C.; Zeng, Q. H.; Yu, A. B. *Nanotechnology* **2006**, *17*, 4929–35. (b) Jiang, X. C.; Zeng, Q. H.; Yu, A. B. *Langmuir* **2007**, *23*, 2218–23. (c) Zeng, Q. H.; Jiang, X. C.; Yu, A. B.; Lu, G. *Nanotechnology* **2007**, *18*, 035708.

(28) (a) Mayor-Lopze, M. J.; Weber, J. *Chem. Phys. Lett.* **1997**, *281*, 226–232. (b) Masel, R. I. *Priciples of Adsorption and Reaction on Solid Surface*; John Wiley and Sons: New York, 1996. (c) Greelings, P.; De Proft, F.; Langenaeker, W. *Chem. Rev.* **2003**, *103*, 1793.

(29) (a) Boon, G.; De Proft, F.; Langenaeker, W.; Geerlings, P. *Chem. Phys. Lett.* **1998**, *295*, 122–128. (b) Boon, G.; Langenaeker, W.; De Proft, F.; De Winter, H.; Tollenaere, J. P.; Geerlings, P. *J. Phys. Chem. A* **2001**, *105*, 8805–8814. (c) Boon, G.; van Alsenoy, C.; De Proft, F.; Bultinck, P.; Geerlings, P. *J. Phys. Chem. A* **2003**, *107*, 11120–27.

(30) Perdew, J. P.; Wang, Y. *Phys. Rev. B* **1986**, *33*, 8800–8802.

(31) Balleto, F.; Ferrando, R. *Rev. Mod. Phys.* **2005**, *77*, 371–423.

JP803935Y